**Title:** Selective *in-vivo* visualization of immune-cell infiltration in a mouse model of autoimmune myocarditis by fluorine-19 cardiac magnetic resonance
**Authors**: Ruud B. van Heeswijk, Jonathan De Blois, Gabriela Kania, Christine Gonzales, Przemyslaw Blyszczuk, Matthias Stuber, Urs Eriksson, and Juerg Schwitter.
**Journal**: Circulation. Cardiovascular Imaging
**Year**: 2013
**Volume**: 6
**Issue**: 2
**Pages**: 277-284
**DOI:** 10.1161/CIRCIMAGING.112.000125

# ***Title Page***

Title

**Selective *in-vivo* visualization of immune-cell infiltration in a mouse model of autoimmune myocarditis by fluorine-19 cardiac magnetic resonance**

Surname and short title: van Heeswijk; Fluorine-19 CMR of myocarditis in mice

Authors

Ruud B. van Heeswijk, PhD*†, Jonathan De Blois, MD¶‡**, Gabriela Kania, PhD§, Christine Gonzales, PhD‡**, Przemyslaw Blyszczuk, PhD§, Matthias Stuber, PhD*†, Urs Eriksson, MD, MSc§†† and Juerg Schwitter, MD‡**.

Affiliations

*Department of Radiology, University Hospital (CHUV) and University (UNIL) of Lausanne, Switzerland, †Center for Biomedical Imaging (CIBM), Lausanne, Switzerland, ¶Centre Hospitalié Affilié Universitaire de Québec, Université Laval, Québec, Canada, ‡Cardiology Service, University Hospital of Lausanne (CHUV), Switzerland, §Cardioimmunology, Cardiovascular Research, Institute of Physiology, University of Zurich, Switzerland, **Cardiac MR Center, University Hospital of Lausanne (CHUV), Switzerland, ††Zurich Regional Health Centre (GZO), Department of Medicine, Wetzikon, Switzerland

Corresponding author

Ruud B. van Heeswijk

CHUV-CIBM

Rue de Bugnon 46, BH 8.84

1011 Lausanne, Switzerland

Tel: +41-21-3147535, Fax: + 41-21-31446 45

e-mail: ruud.mri@gmail.com

Word count: 6050-54=**5998** of 6000 (Abstract up to and including Figure Legends minus Funding)

Journal Subject Codes: 16,30,150

# Abstract

**BACKGROUND:** The goal of this study was to characterize the performance of $^{19}F$ cardiac magnetic resonance (CMR) for the specific detection of inflammatory cells in a mouse model of myocarditis. Intravenously administered perfluorocarbons (PFC) are taken up by infiltrating inflammatory cells and can be detected by fluorine-19 ($^{19}F$) CMR. $^{19}F$-labeled cells should therefore generate an exclusive signal at the inflamed regions within the myocardium.

**METHODS AND RESULTS:** Experimental autoimmune myocarditis (EAM) was induced in BALB/c mice. Following intravenous injection of 2x200µl of a PFC on day 19 and 20 (n=9) after immunization, *in vivo* $^{19}F$-CMR was performed at the peak of myocardial inflammation (day 21). In 5 additional animals, PFC combined with fluorescein isothiocyanate (FITC) was administered for post-mortem immunofluorescence and flow cytometry analyses. Control experiments were performed in 9 animals.

*In vivo* $^{19}F$-CMR detected myocardial inflammation in all EAM-positive animals. Its resolution was sufficient to identify even small inflammatory foci e.g. at the surface of the right ventricle. Post-mortem immunohistochemistry and flow cytometry confirmed the presence of PFC in macrophages, dendritic cells and granulocytes, but not in lymphocytes. The myocardial volume of elevated $^{19}F$ signal ($r_s$=0.96, $p$<0.001), the $^{19}F$ SNR ($r_s$=0.92, $p$<0.001) and the $^{19}F$ signal integral ($r_s$=0.96, $p$<0.001) at day 21 correlated with the histological myocarditis severity score.

**CONCLUSIONS:** *In-vivo* $^{19}F$-CMR was successfully used to specifically and robustly visualize the inflammation in EAM, and thus allowed for an unprecedented insight into the involvement of inflammatory cells in the disease process.



Keywords: magnetic resonance imaging, perfluorocarbon, myocarditis, mouse

# ***Text***

## Introduction

Myocarditis is associated with a broad range of pathological immune processes in the heart[1] and its clinical presentation can vary substantially. Acute myocarditis for example can present with arrhythmias, syncope, or even sudden cardiac death, but it can also progress slowly into a phenotype of inflammatory dilated cardiomyopathy[2]. Cardiac magnetic resonance (CMR) is now accepted as a sensitive method for the work-up of suspected myocarditis[3], e.g. in the setting of acute or chronic heart failure[4]. In addition to the evaluation of cardiac function, CMR allows for tissue characterization by means of the late gadolinium enhancement (LGE) approach, which probes tissue viability, thereby detecting inflammatory lesions when accompanied by irreversible tissue damage[5,6]. CMR can also visualize tissue edema through $T_2$-weighted imaging[7] or more recently by $T_2$ mapping[8]. However, these CMR applications are not specific for a particular type of tissue injury, as necrosis and edema can also develop in the setting of ischemia, e.g. in acute coronary syndrome. In addition, these CMR methods do not provide information on the extent and timing of inflammatory cell infiltrations during the disease process. A non-invasive imaging strategy that detects inflammatory cells and which is not based on secondary tissue alterations (such as necrosis and/or edema) is therefore highly desirable for a more detailed characterization of myocarditis. Ideally, such a technique should exclusively detect inflammation and should be able to do so before alterations in tissue properties even occur. To this end, we investigated a novel CMR approach that is based on the ability of infiltrating inflammatory cells to phagocyte fluorine-containing particles and enables the non-invasive visualization of inflammatory lesions.

Since fluorine ($^{19}F$) is virtually absent in animals and humans, $^{19}F$ magnetic resonance imaging (MRI) offers the unique possibility to detect an injected substance that contains $^{19}F$ without any background signal

and with 85% of the sensitivity of $^{1}$H MRI[9]. This theoretically results in a very high contrast-to-noise ratio (CNR) and a high specificity of the signal, as any $^{19}$F signal detected in the body can be unambiguously attributed to the injected $^{19}$F. As the signal received by an MR volume coil is directly proportional to the amount of $^{19}$F nuclei present in the tissue, the signal can be related to a reference of known $^{19}$F concentration, which renders this technique fully quantitative[10]. In this regard it differs from 'indirect' contrast agents that are based on relaxation time alterations (such as iron oxide or gadolinium), which often have a non-linear dose-signal response at higher concentrations[11]. Finally, the $^{19}$F signal can be fused with conventional $^{1}$H images for anatomical co-registration[12]. As demonstrated by several groups[13], $^{19}$F MRI is able to detect macrophages after intravenous injection of PFC emulsions in several disease processes, such as pneumonia[14], heterotopic acute cardiac allograft rejection in rat and in mouse models[15,16], and in healing after myocardial infarction in mice[17].

The goal of the present study was therefore to characterize the performance of $^{19}$F-CMR for the specific detection of inflammatory cells in a mouse model of $CD4^{+}$ T-cell-mediated autoimmune myocarditis (EAM)[18]. EAM tends to progress into an inflammatory dilated cardiomyopathy (iDCM) phenotype along with development of increased interstitial fibrosis. In the EAM model quantifiable stages of acute myocarditis and iDCM can be distinguished[19]. EAM thus appears to be an ideal model to test the hypothesis that $^{19}$F-CMR is able to detect the inflammatory cells recruited to the myocardium of EAM mice both non-invasively and quantitatively. In the setting of an inflammatory process, currently available MR methods allow for the measurement of necrosis, edema, fibrosis, and alterations of regional or global function. The proposed $^{19}$F-based CMR approach may provide complementary information related to the disease process itself, i.e. the amount and timing of myocardial infiltration by inflammatory cells, which could advance our understanding of the inflammatory disease process and may also enable an early detection of the disease.

# Methods

### Experimental Autoimmune Myocarditis Model

All animal experiments performed in this study were approved by the local and institutional animal ethics committee. A total of 23 male BALB/c mice (29.4±3.2g) entered the study (Figure 1). To induce experimental autoimmune myocarditis (EAM), 17 mice were injected subcutaneously with 150μg of αMyHC peptide (Ac-RSLKLMATLFSTYASADR-OH; Caslo, Lyngby, Denmark) emulsified 1:1 with Complete Freund's Adjuvant (CFA, Difco, Franklin Lakes, NJ) on days 0 and 7, as previously described[20]. In the EAM model, immunization results in acute myocarditis that peaks approximately 21 days after immunization. Inflammation resolves slowly thereafter, while the number of cardiac fibroblasts progressively increases on follow-up[21]. Six mice were sham-immunized with saline/CFA and served as controls.

### *In vivo* Inflammatory-Cell Labeling

The main $^{19}$F *in-vivo* cellular labeling agent used in this study in 9 EAM mice was an emulsion of a linear polymer PFC (V-Sense 1000H, Celsense, Pittsburgh, PA, USA) that contains $1.67\times10^{24}$ $^{19}$F atoms per liter. Furthermore, 5 additional EAM mice were injected with a dual-labeled PFC that also contains FITC (fluorescein isothiocyanate) for post-mortem fluorescent microscopy and flow-cytometry analyses. This dual-labeling FITC-PFC is known to remain stable without dissociation of its components for over a week in cell cultures, while it is also characterized by a slightly decreased labeling efficiency versus the non-fluorescent compound (unpublished data, provided by the manufacturer) and was thus not used in MR signal calculations. The PFC emulsion was administered through the tail vein at a dose of 200μL (6.8ml/kg body weight) on both day 19 and 20 after immunization (Figure 1). Three EAM mice served as controls and were injected with saline instead of PFC before $^{19}$F-CMR.

**$^{1}$H and $^{19}$F-CMR**

On day 21 after immunization, animals underwent isoflurane anesthesia. The animals were placed on top of a custom-designed 18mm-diameter quadrature surface coil tunable to both the $^{1}$H and $^{19}$F frequencies (400.2 and 376.6 MHz, respectively). The body temperature was monitored and kept constant at 37.0±0.5°C. A respiration-gated and ECG-triggered segmented k-space gradient echo sequence (repetition time TR=3.8ms, echo time TE=1.9ms, 4 signal averages, 128x128 matrix, 30x30mm$^2$ field of view (FoV), slice thickness 2mm, total acquisition time ~5min) was used (9.4T spectrometer, Varian, Palo Alto, CA) to obtain three $^{1}$H short-axis images of the heart. At the anatomical location of the central slice, a prospectively gated gradient-echo cine imaging series (TR=10ms, TE=1.9ms, 14 frames, 4 signal averages, 128x128 matrix, slice thickness 1mm, total acquisition time ~5min) was also acquired. Next, at the location of the 3 $^{1}$H short-axis images, a turbo spin echo sequence (TR=500ms, TE=3.7ms, echo-train length 4, 240 signal averages, 64x64 matrix, total acquisition time 32min) was used for the $^{19}$F-CMR acquisitions.

After the *in-vivo* CMR acquisitions, the animals were sacrificed with pentobarbital and the hearts were perfused with saline, excised and fixed in formalin for post-mortem analysis. To investigate whether the *in-vivo* $^{19}$F signal was related to the proximity of the RF coil to the anterior wall of the heart, e*x-vivo* high-resolution $^{1}$H- and $^{19}$F-CMR of the hearts of 7 mice (Figure 1A) placed with their apex closest to the RF coil was performed. A 3D gradient echo sequence (TR=7.0ms, TE=3.6ms, 256 signal averages, 128×128×64 matrix, FoV 15×15×15mm$^3$, acquisition time: 4h4min), which had better spatial coverage but inferior sensitivity per unit of time than the *in-vivo* sequence, was used.

All image analyses were performed on the unprocessed modulus images in Matlab (Mathworks, Natick, MA, USA). The total myocardial volume with elevated $^{19}$F signal ($Vol_{inflam}$) was determined as follows (for details, see Supplemental Figure 1): first, the heart and the liver were segmented on the anatomic $^{1}$H images. Next, the liver was segmented in the corresponding $^{19}$F images, while the $^{19}$F noise level was determined as the standard deviation of the $^{19}$F signal intensity of a large region outside the mouse body. Finally, the voxels of the $^{19}$F images that were in the region of the heart but not in the liver and had a $^{19}$F signal 7 times higher

than the noise were added up to $Vol_{inflam}$ and their average signal-to-noise ratio (SNR) was calculated. This threshold for detection of $^{19}F$-positive pixels was applied to avoid pixel selection in minor motion-related ghosts and the isoflurane anesthetic that were consistently lower in signal than this threshold. The $^{19}F$ signal integral was then calculated as the product of $Vol_{inflam}$ and the SNR. To study the prevalent spatial distribution of the $^{19}F$ signal in EAM[6], the *in-vivo* $^{19}F$ signal distribution of each animal was classified in analogy to the standard myocardial segmentation model[22], but without the apical segment and with six additional segments covering the right ventricle. A segment was defined positive if ≥25% of pixels of the segment showed an elevated $^{19}F$ signal. The LV area shortening fraction was calculated from end-diastolic and end-systolic $^{1}H$ cine images acquired at the mid-ventricular level (Argus, Siemens Healthcare, Erlangen, Germany) as a rough estimate for global LV systolic function.

A dilution series of the PFC in agar was created to ascertain the minimum $^{19}F$ atomic concentration needed for its detection with the *in-vivo* pulse sequence at a given SNR=2.

**Histology, Immunohistochemistry and Immunofluorescence**

The inflammatory cell infiltrations of the excised hearts mentioned above were analyzed in paraffin sections (Figure 1). Adjacent heart sections were treated differently in order to determine 1) the myocarditis severity score with hematoxylin-eosin (HE), 2) the cell type in the inflammatory cell area by immunohistochemistry and 3) the presence of PFC-FITC in inflammatory cells by immunofluorescence.

The myocarditis severity was scored as described previously[19] on the HE-stained heart sections using a semi-quantitative scale: 0 – no inflammatory infiltrates; 1 – small foci of inflammatory cells between myocytes; 2 – larger foci of >100 inflammatory cells; 3 – >10% of a cross-section involved; 4 – >30% of a cross-section involved[19]. Correlations were calculated between this histological disease score and the $^{19}F$ SNR, $Vol_{inflam}$, the signal integral, and the midventricular LV area shortening fraction.

For immunohistochemistry, rabbit anti-mouse CD45 1:250 (BD Bioscience, Switzerland) and rat anti-mouse F4/80 1:150 (BMA Biomedicals, Switzerland) antibodies were used to detect inflammatory bone marrow-

derived cells and macrophages, respectively. Diaminobenzidine (DAB) was used as the chromogen. For immunofluorescence, rat-anti-F4/80 1:100 (Abcam, Boston, MA, USA) and monoclonal rabbit-anti-FITC 1:100 (Invitrogen, Switzerland) were used to detect macrophages and PFC-FITC, respectively. The fluorochrome-conjugated secondary antibodies used were Alexa 546 goat-anti-rat 1:600 and Alexa 488 chicken-anti-rabbit, respectively (Invitrogen). Nuclei were detected with DAPI (Roche, Switzerland).

**Flow cytometry**

Hearts from FITC-PFC-injected EAM mice (Figure 1C) were excised at day 21 after immunization, then perfused with cold PBS, dissected into small pieces and digested for 50min at 37°C in collagenase blendzyme (Liberase; Roche, Switzerland). Single cell suspensions were obtained by straining through a 70µm nylon mesh (BD Biosciences). Cells were washed twice with 50mL FACS buffer (1% FCS, 1 mM EDTA in phosphate buffered saline-PBS, all from Gibco, Switzerland) and incubated 30 minutes on ice with the appropriate combination of fluorochrome- or biotin-conjugated antibodies. The following antibodies were used: fluorochrome-conjugated antibodies: anti-CD45-PE, anti-CD11b-APC, anti-CD11c-APC, anti-CD4-APC, anti-Gr-1-PE (all from BD Bioscience), biotin-conjugated antibodies: anti-F4/80 (Cedarlane, Burlington, ON, Canada), anti-CD45 (BD Bioscience). Streptavidin-APC (BD Bioscience) was used to detect biotin-conjugated antibodies. Cells were profiled with the FACS-Canto analyzer (BD Bioscience) and data were analyzed with FlowJo software (Tree Star, Ashland, OR).

**Statistical analyses**

All statistical analyses were made in SPSS Statistics 20.0 (IBM, Armonk, NY), The groups of EAM and control mice were compared with unpaired two-tailed Student's t-tests. Correlations of the $^{19}$F-SNR, $Vol_{inflam}$, $^{19}$F signal integral and LV area shortening with the disease severity score were calculated with Spearman's ranked correlation. $p<0.05$ was considered significant.

# Results

EAM was induced in 17 animals as confirmed in 11 animals by histology (Figure 1, experiments A,C,D). In the 3 animals used for flow cytometry, histology was not applicable, while in another 3 animals histology was not performed for technical/logistical reasons. No adverse effects were observed after PFC injections in any of the experiments.

### Detection of EAM by $^{19}$F-CMR

*In-vivo* CMR of PFC-injected mice with myocarditis demonstrated $^{19}$F signal in all 9 animals (see for example Figure 2, solid arrows). $^{19}$F-positive regions in the heart were well defined and showed a predilection of the sub-epicardial layers of the myocardium as illustrated in Figure 2C and 2D (inferior LV wall). Three-dimensional high-resolution *ex-vivo* CMR confirmed the predominantly subepicardial distribution of the $^{19}$F signal (n=10, from experiments A(n=7) and B(n=3)). An example is shown in Figure 3.

In the in vivo experiments, a $^{19}$F signal was furthermore observed in the liver (Figure 2, dotted arrows) and was attributed to PFC phagocytosed by Kuppfer cells[23]. This liver signal was also observed in the six sham-immunized PFC-injected control animals without myocarditis (Figure 2F), while no $^{19}$F signal was detected in their hearts.

A diffuse low-intensity $^{19}$F signal that was ascribed to the anesthetic isoflurane was observed in the subcutaneous fat in most animals, but was usually removed by the processing threshold. The SNR of the $^{19}$F signal regions in the heart was 25±19 (range: 4 to 60), while $Vol_{inflam}$ was 46±46mm$^3$ (range: 7 to 144mm$^3$).

The distribution of the average $^{19}$F signal (n=11, experiments A,C) was located predominantly in the basal anterolateral part of the heart, while the $^{19}$F signal was completely absent in the inferior and inferoseptal segments (Figure 4).

The PFC dilution series showed an SNR~2 at a $^{19}F$ concentration of ~10mM, which indicated that the post-processing threshold cut off $^{19}F$ concentrations lower than 35mM (7 times the standard deviation of the noise) or 15.4nmol/voxel.

**Co-localization of inflammatory cells and $^{19}F$ signal in the inflamed myocardium**

Immunohistochemistry confirmed the presence of CD45 and F4/80-positive inflammatory cells in the heart at locations where the $^{19}F$ signal was observed by CMR (Figure 5). In the mice injected with the dual-labeled emulsion, fluorescent microscopy demonstrated co-localization of the F4/80 marker (macrophage) and FITC (PFC) signal (Figure 6) and thus F4/80-positive macrophages were identified as a source of the $^{19}F$ signal.

**Incorporation of PFC emulsion in different cells infiltrating the myocardium**

To determine which cell types were able to incorporate the PFC-FITC emulsion in the inflammatory environment of the heart, flow cytometry analysis of FITC (which corresponded to PFC) was performed on non-myocyte single cell populations isolated from the myocardium of the EAM mice that were injected with the PFC-FITC emulsion. FITC was detected in CD45+/CD11b+ monocytes, CD45+/F4/80+ macrophages, CD45+/CD11c+ dendritic cells and CD45+/Gr-1+ granulocytes. While this EAM model is known to be mediated by CD4+ lymphocytes[19], no FITC was detected in CD45+/CD4+ T-lymphocytes (Figure 7).

**Correlation of histological disease score and CMR parameters**

A significant correlation was found between the histological disease severity score and the SNR of the $^{19}F$ signal ($r_s$=0.92, $p$<0.001) as well as $Vol_{inflam}$ ($r_s$=0.96, p<0.001) and the $^{19}F$ signal integral ($r_s$=0.96, $p$<0.001), as demonstrated in Figure 8. In contrast, the midventricular LV area shortening fraction, which was used as an estimate of LV systolic function, did not correlate with the disease score ($r_s$=-0.14, $p$=0.65).

The average midventricular LV area shortening fraction in the healthy animals was 72.2±5.5% (vs EAM mice: 66.2±8.3%, $p$=0.38).

# Discussion

### *In-vivo* detection of inflammatory cell infiltration in EAM by $^{19}$F-CMR

To our knowledge, this pre-clinical study for the first time shows that *in-vivo* CMR is able to detect inflammatory infiltrations in a model of experimental autoimmune myocarditis. In the beating mouse heart, the spatial and temporal resolution of the $^{19}$F-CMR acquisitions was sufficiently high to detect immune cells in thin myocardial structures such as the surface of the left and right ventricular free walls as shown in Figure 2 and 5. In addition, the $^{19}$F signal was sufficiently specific to yield a close correlation with the histological disease severity. This $^{19}$F-CMR approach thus yields information on the myocardial inflammatory cell infiltration in myocarditis. Consequently, it expands our current armamentarium to characterize myocarditis by adding this information to that on necrosis, edema, fibrosis, and function that can already be obtained by conventional CMR techniques.

The EAM model shares several similarities with human inflammatory heart disease, such as relapses, the development of interstitial fibrosis, cardiac dilation and heart failure over time[21]. In the current in-vivo and particularly in the ex-vivo experiments, inflammatory infiltrates were predominantly observed in the subepicardial layers of the myocardium, which resembles the distribution of tissue damage in human viral myocarditis[24]. Similar to humans, the most prevalent location of inflammation in the mice with EAM was the base of the LV. However, in the animal model the predilection site for inflammation was found in the antero-lateral wall, while in humans the predilection site is typically the infero-lateral wall of the LV.

### Confirmation of infiltrating inflammatory cells as source of $^{19}$F signal in EAM

Since the PFC emulsion was injected intravenously to detect inflammation in the heart, it is crucial to determine into which cell types the PFC was incorporated in the *in-vivo* situation. While the immunostaining for CD45 and F4/80 was mainly detected in the subepicardial layers as was the $^{19}$F signal, this finding in

itself does not prove PFC incorporation into macrophages. Therefore, we used a PFC combined with FITC to co-localize its fluorescence within macrophages (Figure 5), which was not found in the controls. Finally, flow cytometry demonstrated incorporation of the PFC-FITC emulsion into F4/80+ macrophages, Gr-1+ granulocytes, CD11c+ dendritic cells, and CD11b+ monocytes. While the EAM model is mediated by CD4+ lymphocytes, no PFC-FITC incorporation was found in this cell population. Thus, these results support the notion that intravenously administered PFC in the EAM model yield $^{19}F$ signals originating mainly from infiltrating inflammatory cells. In a model of LPS-induced pneumonia[14] and in inflammation following cardiac and cerebral ischemia[17], PFC was detected predominantly in the monocyte/macrophage and dendritic cell fractions and to a lesser extent in neutrophils, while T-cells did not incorporate the PFC. Thus, these and other data[15,25] are well in line with our current findings in the EAM model.

**Study Limitations**

The use of a surface coil in this study yielded a high detection sensitivity for $^{19}F$, while it removed the option of direct fluorine quantification through comparison with an external reference phantom. For absolute quantification, a volume coil would be required in combination with a reference of known $^{19}F$ concentration. Conversely, by using array coils or compressed sensing[26] the received signal per unit of time could possibly be amplified several times compared to that obtained by the coil used in our experiments, thus allowing for shorter acquisition times and/or higher detection sensitivity.

Of note, no correlation was found between the midventricular LV area shortening fraction estimate and the disease score. This is not surprising, given that in the EAM model heart failure develops after the peak of acute inflammation, in most cases not earlier than 30 to 50 days after immunization. Nevertheless, as the area shortening fraction was calculated from a single mid-ventricular slice and not from the entire LV, we cannot entirely exclude that a correlation would exist if function of the entire LV had been measured.

Since PFCs are inert molecules, their elimination from the body is unlikely to cause toxicity concerns[27]. However, this aspect will require additional in-depth studies in the future. At the current stage, the minimum

required PFC dose for mocarditis detection by $^{19}$F-CMR is not yet known. Lower dosages than those used in this study may still be critically enabling for monitoring inflammatory cell infiltration and/or responsiveness to therapy by the PFC used in this study. Furthermore, for the method to be clinically useful, further studies are needed to demonstrate the ability to detect inflammation at earlier stages of myocarditis. In particular, the lack of PFC uptake by lymphocytes might decrease the sensitivity of this approach to detect early stages of myocarditis.

**Clinical perspective – Applications in humans**

In the current *in-vivo* study, the SNR of the $^{19}$F positive heart regions was high (25±19) with a voxel size of 0.47x0.47x2mm$^3$ acquired over 32min at 9.4T. Current voxel sizes in human studies to detect e.g. small necrotic lesions in myocarditis are in the order of 2x2x8mm$^3$. Thus, with a 72-times larger voxel size in humans, a similar SNR for $^{19}$F could theoretically be obtained at 3T (instead of 9.4T) with a 7-minute acquisition. This rough estimate does not account for any improvements in pulse sequences and coil designs that may be exploited if such a $^{19}$F-based approach were further pursued on commercial human MRI scanners. Thus, transition of this $^{19}$F-CMR approach into the human setting appears to be in reach from a technical point of view. In addition, the PFC compounds are inert molecules and some of them have already passed safety trials in humans when used as potential plasma expanders[27]. When PFCs were used for *in-vitro* labeling experiments, no negative effects were found on cell viability and cell function of dendritic cells[28] and polymorphonuclear neutrophils[29]. In summary, these current and other preliminary results of $^{19}$F MRI applications for inflammation detection and the fact that the PFCs exhibit a high safety profile[27-29], suggest a feasible and highly desirable transition of this $^{19}$F approach into a clinical application. From a biological point of view, future studies are needed to test whether human macrophages are able to incorporate PFC *in-vivo* in sufficient quantities to allow for non-invasive detection by $^{19}$F-CMR.

In addition, conventional $^{1}$H anatomical images can easily be fused with the $^{19}$F images, which allows for an exact co-registration of the $^{19}$F signal with cardiac anatomy. Conventional $^{1}$H CMR can be applied in

the same session to assess myocardial global and regional function, cardiac remodeling, myocardial edema, perfusion, and necrosis.

Currently, the ability to detect myocarditis by conventional $^{1}$H CMR through secondary tissue alterations such as edema and necrosis is clinically highly valuable. However, the prospect of being able to non-invasively, quantitatively, and specifically visualize the early-stage recruitment of immune cells into the myocardium with a $^{19}$F-CMR approach could represent an important step towards a better understanding of the pathophysiology of myocarditis. It could also allow for early detection of the disease and it potentially opens opportunities for treatment monitoring of myocarditis. Longitudinal studies combining $^{1}$H- and $^{19}$F-CMR could be used to assess the timing of inflammatory cell infiltration, development of edema and necrosis, alterations in function, and finally transition of myocarditis into various phenotypes such as e.g. dilated cardiomyopathy with local[24] or interstitial[30] fibrosis development.

## Conclusions

In this study, $^{19}$F-CMR was successfully applied in a mouse model of experimental autoimmune myocarditis to specifically and robustly visualize the inflammation process of myocarditis. This critically enabled an unprecedented insight into the involvement of inflammatory cells in the disease process. This approach can provide novel information on the magnitude and the timing of inflammatory cell infiltration in myocarditis and may add potentially valuable information complementary to that on necrosis, edema, fibrosis, and function obtained by conventional CMR methods.

# Acknowledgements

# Funding Sources

This work was supported by the Centre d'Imagerie BioMédicale (CIBM) of the UNIL, UNIGE, HUG, CHUV, EPFL and the Leenaards and Jeantet Foundations. Jonathan De Blois was supported by a bursary award from Université Laval (Quebec City, Canada). Gabriela Kania and Urs Eriksson acknowledge support from the Swiss National Foundation grant 32003B_130771.


# Disclosures

None.

# References


1. Sagar S, Liu PP, Cooper LT, Jr. Myocarditis. *Lancet*. 2012;379:738-747
2. Kawai C. From myocarditis to cardiomyopathy: Mechanisms of inflammation and cell death: Learning from the past for the future. *Circulation*. 1999;99:1091-1100
3. Friedrich MG, Sechtem U, Schulz-Menger J, Holmvang G, Alakija P, Cooper LT, White JA, Abdel-Aty H, Gutberlet M, Prasad S, Aletras A, Laissy JP, Paterson I, Filipchuk NG, Kumar A, Pauschinger M, Liu P. Cardiovascular magnetic resonance in myocarditis: A jacc white paper. *J Am Coll Cardiol*. 2009;53:1475-1487
4. McMurray JJ, Adamopoulos S, Anker SD, Auricchio A, Bohm M, Dickstein K, Falk V, Filippatos G, Fonseca C, Sanchez MA, Jaarsma T, Kober L, Lip GY, Maggioni AP, Parkhomenko A, Pieske BM, Popescu BA, Ronnevik PK, Rutten FH, Schwitter J, Seferovic P, Stepinska J, Trindade PT, Voors AA, Zannad F, Zeiher A. Esc guidelines for the diagnosis and treatment of acute and chronic heart failure 2012. *Eur Heart J*. 2012;33:1787-1847
5. Simonetti OP, Kim RJ, Fieno DS, Hillenbrand HB, Wu E, Bundy JM, Finn JP, Judd RM. An improved mr imaging technique for the visualization of myocardial infarction. *Radiology*. 2001;218:215-223
6. Mahrholdt H, Goedecke C, Wagner A, Meinhardt G, Athanasiadis A, Vogelsberg H, Fritz P, Klingel K, Kandolf R, Sechtem U. Cardiovascular magnetic resonance assessment of human myocarditis: A comparison to histology and molecular pathology. *Circulation*. 2004;109:1250-1258
7. Friedrich MG. Myocardial edema--a new clinical entity? *Nat Rev Cardiol*. 2010;7:292-296

8. Thavendiranathan P, Walls M, Giri S, Verhaert D, Rajagopalan S, Moore S, Simonetti OP, Raman SV. Improved detection of myocardial involvement in acute inflammatory cardiomyopathies using t2 mapping. *Circ Cardiovasc Imaging*. 2012;5:102-110
9. Ahrens ET, Flores R, Xu H, Morel PA. In vivo imaging platform for tracking immunotherapeutic cells. *Nature biotechnology*. 2005;23:983-987
10. Srinivas M, Turner MS, Janjic JM, Morel PA, Laidlaw DH, Ahrens ET. In vivo cytometry of antigen-specific t cells using 19f mri. *Magn Reson Med*. 2009;62:747-753
11. Shahbazi-Gahrouei D, Williams M, Allen BJ. In vitro study of relationship between signal intensity and gadolinium-dtpa concentration at high magnetic field strength. *Australas Radiol*. 2001;45:298-304
12. Joseph PM, Fishman JE, Mukherji B, Sloviter HA. In vivo 19f nmr imaging of the cardiovascular system. *J Comput Assist Tomogr*. 1985;9:1012-1019
13. Temme S, Bonner F, Schrader J, Flogel U. 19f magnetic resonance imaging of endogenous macrophages in inflammation. *Wiley Interdiscip Rev Nanomed Nanobiotechnol*. 2012;4:329-343
14. Ebner B, Behm P, Jacoby C, Burghoff S, French BA, Schrader J, Flogel U. Early assessment of pulmonary inflammation by 19f mri in vivo. *Circ Cardiovasc Imaging*. 2010;3:202-210
15. Hitchens TK, Ye Q, Eytan DF, Janjic JM, Ahrens ET, Ho C. 19f mri detection of acute allograft rejection with in vivo perfluorocarbon labeling of immune cells. *Magn Reson Med*. 2011;65:1144-1153
16. Flogel U, Su S, Kreideweiss I, Ding Z, Galbarz L, Fu J, Jacoby C, Witzke O, Schrader J. Noninvasive detection of graft rejection by in vivo (19) f mri in the early stage. *Am J Transplant*. 2011;11:235-244
17. Flogel U, Ding Z, Hardung H, Jander S, Reichmann G, Jacoby C, Schubert R, Schrader J. In vivo monitoring of inflammation after cardiac and cerebral ischemia by fluorine magnetic resonance imaging. *Circulation*. 2008;118:140-148
18. Eriksson U, Kurrer MO, Sonderegger I, Iezzi G, Tafuri A, Hunziker L, Suzuki S, Bachmaier K, Bingisser RM, Penninger JM, Kopf M. Activation of dendritic cells through the interleukin 1 receptor 1 is critical for the induction of autoimmune myocarditis. *J Exp Med*. 2003;197:323-331
19. Marty RR, Dirnhofer S, Mauermann N, Schweikert S, Akira S, Hunziker L, Penninger JM, Eriksson U. Myd88 signaling controls autoimmune myocarditis induction. *Circulation*. 2006;113:258-265
20. Eriksson U, Kurrer MO, Schmitz N, Marsch SC, Fontana A, Eugster HP, Kopf M. Interleukin-6-deficient mice resist development of autoimmune myocarditis associated with impaired upregulation of complement c3. *Circulation*. 2003;107:320-325
21. Blyszczuk P, Kania G, Dieterle T, Marty RR, Valaperti A, Berthonneche C, Pedrazzini T, Berger CT, Dirnhofer S, Matter CM, Penninger JM, Luscher TF, Eriksson U. Myeloid differentiation factor-88/interleukin-1 signaling controls cardiac fibrosis and heart failure progression in inflammatory dilated cardiomyopathy. *Circ Res*. 2009;105:912-920
22. Cerqueira MD, Weissman NJ, Dilsizian V, Jacobs AK, Kaul S, Laskey WK, Pennell DJ, Rumberger JA, Ryan T, Verani MS. Standardized myocardial segmentation and nomenclature for tomographic imaging of the heart. *Circulation*. 2002;105:539-542
23. Mattrey RF, Scheible FW, Gosink BB, Leopold GR, Long DM, Higgins CB. Perfluoroctylbromide: A liver/spleen-specific and tumor-imaging ultrasound contrast material. *Radiology*. 1982;145:759-762
24. Mahrholdt H, Wagner A, Deluigi CC, Kispert E, Hager S, Meinhardt G, Vogelsberg H, Fritz P, Dippon J, Bock CT, Klingel K, Kandolf R, Sechtem U. Presentation, patterns of myocardial damage, and clinical course of viral myocarditis. *Circulation*. 2006;114:1581-1590

25. Hertlein T, Sturm V, Kircher S, Basse-Lusebrink T, Haddad D, Ohlsen K, Jakob P. Visualization of abscess formation in a murine thigh infection model of staphylococcus aureus by 19f-magnetic resonance imaging (mri). *PLoS One*. 2011;6:e18246
26. Zhong J, Mills PH, Hitchens TK, Ahrens ET. Accelerated fluorine-19 mri cell tracking using compressed sensing. *Magn Reson Med*. 2012, Jul 26. doi: 10.1002/mrm.24414. [Epub ahead of print]
27. Riess JG. Perfluorocarbon-based oxygen delivery. *Artif Cells Blood Substit Immobil Biotechnol*. 2006;34:567-580
28. Bonetto F, Srinivas M, Heerschap A, Mailliard R, Ahrens ET, Figdor CG, de Vries IJ. A novel (19)f agent for detection and quantification of human dendritic cells using magnetic resonance imaging. *Int J Cancer*. 2011;129:365-373
29. Haufe D, Koenigshausen E, Knels L, Wendel M, Stehr SN, Koch T. Leukocyte antibacterial functions are not impaired by perfluorocarbon exposure in vitro. *Am J Physiol-Lung C* 2008;295:L134-142
30. Ugander M, Oki AJ, Hsu LY, Kellman P, Greiser A, Aletras AH, Sibley CT, Chen MY, Bandettini WP, Arai AE. Extracellular volume imaging by magnetic resonance imaging provides insights into overt and sub-clinical myocardial pathology. *Eur Heart J*. 2012;33:1268-1278

# *Figure Titles and Legends*

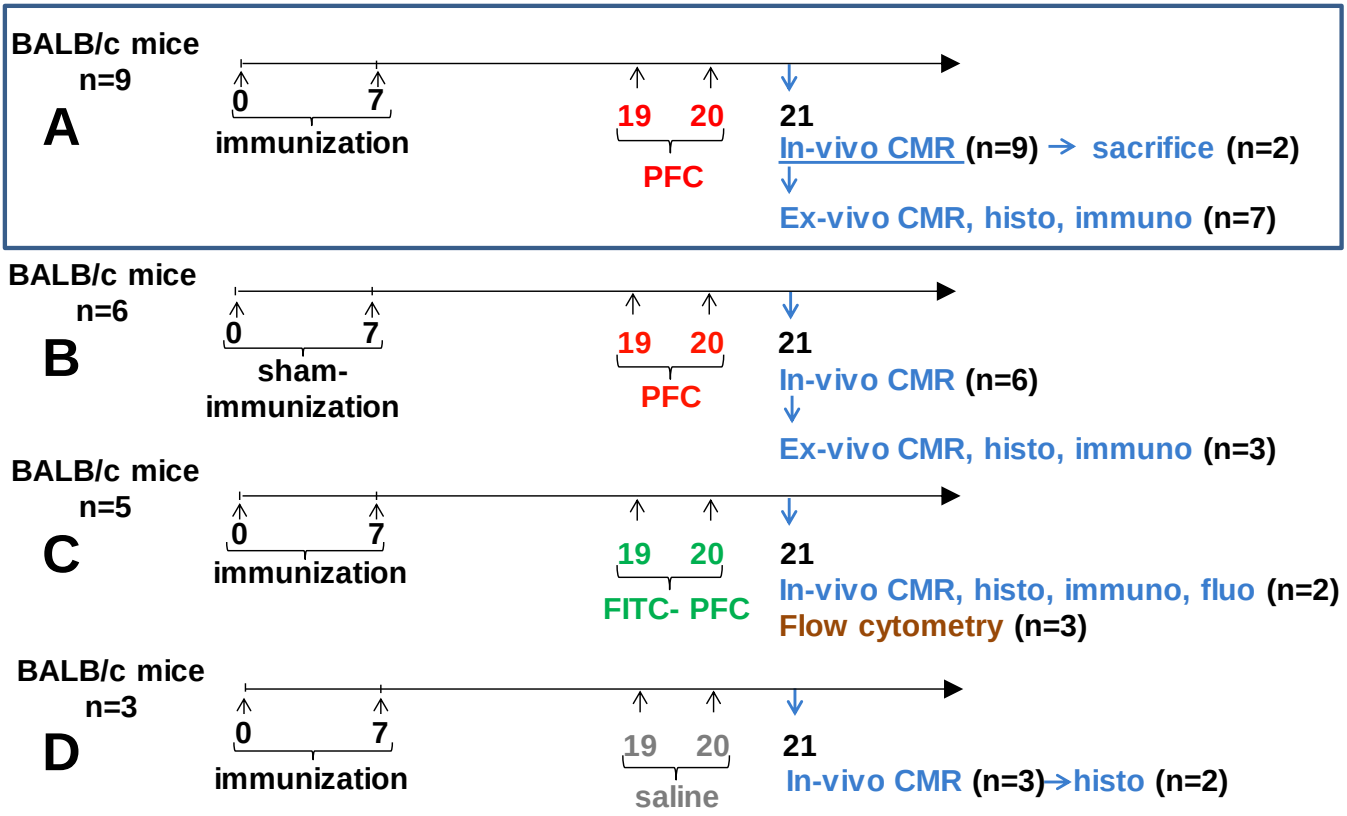


**Figure 1. Overview of the time scale of the different experimental procedures.** Time advances from left to right and is indicated in days, while a number of animals X that und

ergoes a certain procedure is given as n=X. **A)** For the principal investigation, n=9 mice were immunized to develop EAM and were subsequently injected with PFC. They were then sacrificed, after which n=7 excised mouse hearts received ex-vivo CMR, histology ('histo') and immunohistology ('immuno'). **B)** n=6 mice served as healthy controls (disease grade 0). They were sham-immunized but received PFC injections. They were also used in the correlation calculations shown in Figure 8. **C)** n=5 mice received the dual-labeled FITC-PFC instead of PFC. n=2 of these mice were used for co-localization of the PFC with macrophages through immunofluorescence ('fluo'), while n=3 animals were used for flow cytometry to investigate which type of immune cells in the myocardium had phagocytized the PFC. **D)** n=3 mice were immunized to induce

EAM but were injected with saline instead of PFC to assure that there were no $^{19}$F MR signals in the heart if no PFC was injected.

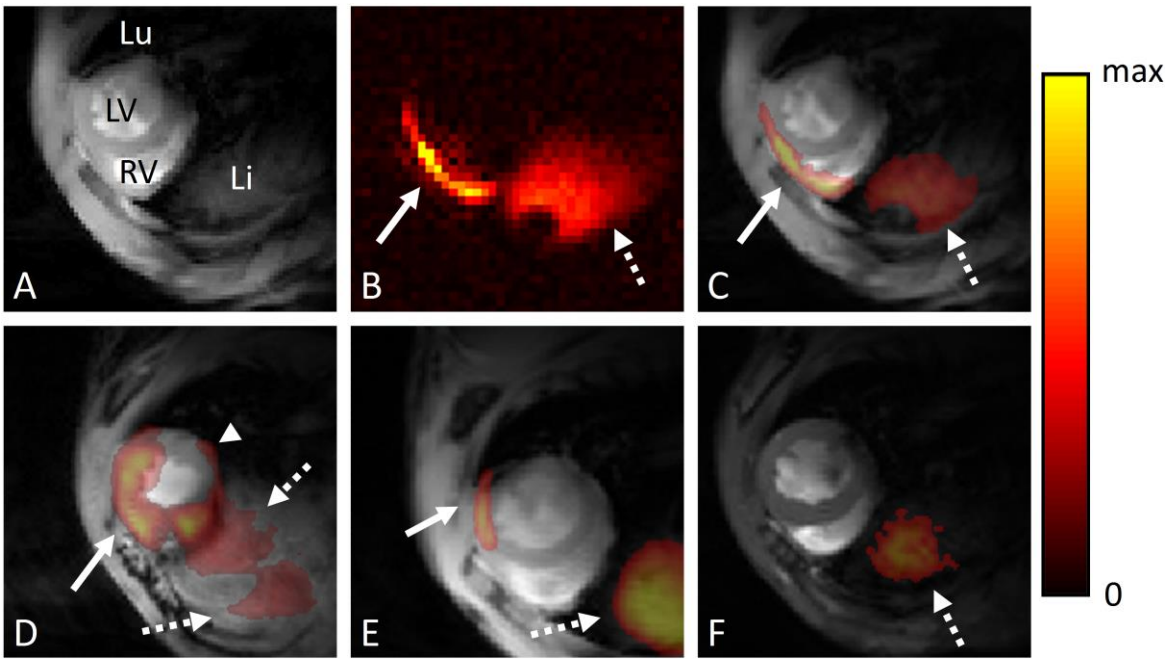


**Figure 2.** ***In vivo*** **$^{19}$F-CMR of myocarditis. (A)** $^{1}$H CMR slice in the short-axis orientation at the base of the heart of a mouse with disease score 3; $^{1}$H CMR depicts the right and left ventricles (RV and LV) as well as the lung (Lu) and liver (Li). **(B)** $^{19}$F-CMR of the same anatomical location. Two regions with a $^{19}$F signal can be observed: a thin line at the level of the myocardium (solid arrow) and a larger region at the level of the liver (dotted arrow). The color coding for $^{19}$F signal intensity is given to the right (in arbitrary units). **(C)** Fusion of the $^{1}$H (A) and $^{19}$F images (B): the $^{19}$F signal co-localizes with the subepicardial layer of the LV anterior wall, the RV free wall (arrow) and the liver (dotted arrow). **(D)** A similar fused basal slice in an animal with disease score 4. Here, the $^{19}$F signal is spread over the majority of the ventricles with a subepicardial $^{19}$F signal in the inferior wall of the LV (arrow head). **(E)** Animal with disease score 2 with a relatively small patch of $^{19}$F signal (arrow). **(F)** Healthy control, in which a $^{19}$F signal can only be observed in the liver (dotted arrow).

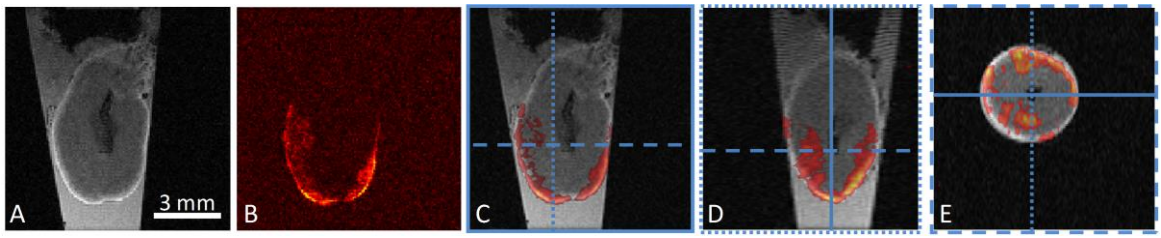


**Figure 3. Three-dimensional *ex vivo* CMR of a mouse heart with myocarditis. (A)** Anatomical $^{1}$H long-axis MR image of the heart, sacrificed at day21 in an Eppendorf tube. **(B)** $^{19}$F MR image at the same anatomical location with the same resolution of 112×112×224μm$^{3}$ as for the $^{1}$H image. **(C)** Fusion image demonstrating the $^{19}$F signal in the subepicardial layer of the LV. The blue lines indicate the location at which the orthogonal images in **(D&E)** are located. The pattern of the frames of the last three images (solid, dashed and dotted line) corresponds to the image orientations as shown by the corresponding cross-sectional line patterns.

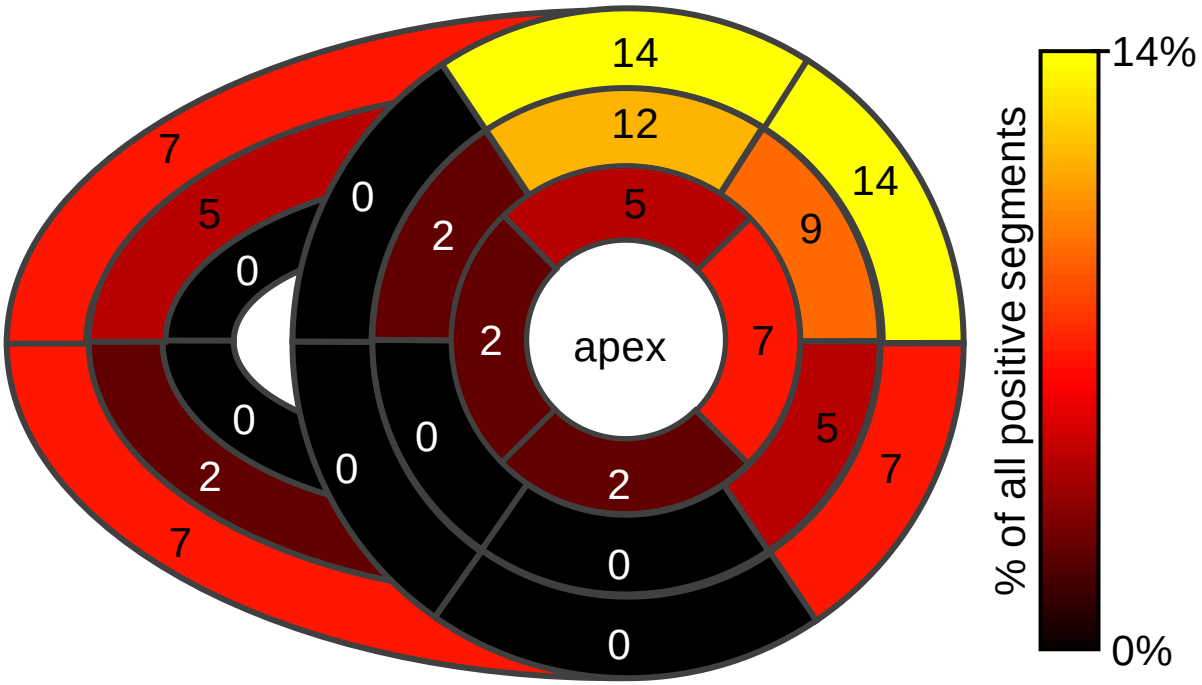


**Figure 4. Distribution of the average $^{19}$F signal over the standard myocardial segmentation.** The concentric rings represent the basal, mid-ventricular and apical slices. A clear prevalence for the basal anterior and basal anterolateral segments can be observed. Interestingly, the $^{19}$F-CMR was also able to detect a significant $^{19}$F signal contribution from segments in the right ventricle. The percentage represents the

portion of the total of $^{19}$F-positive segments determined in n=11 animals (9 from experiment A and 2 from experiment C).

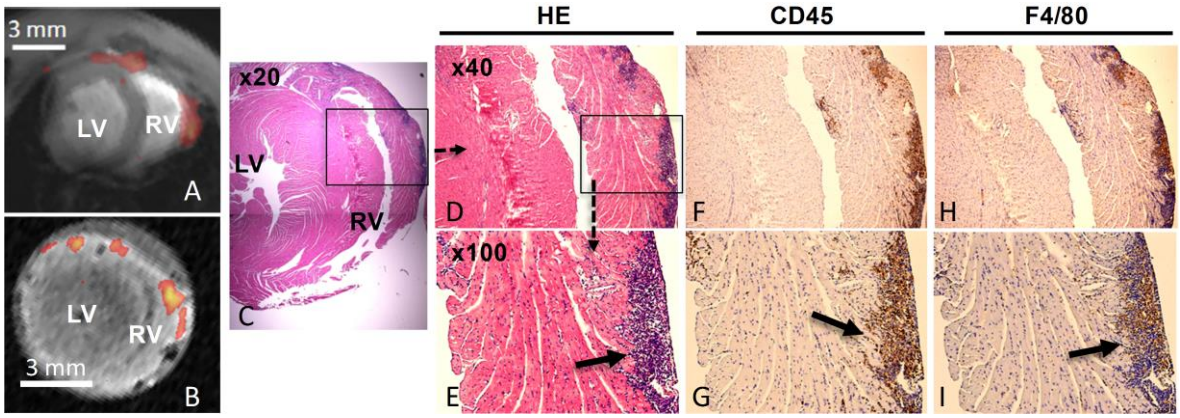


**Figure 5. Histological confirmation of inflammatory cell infiltration at the site of $^{19}$F-CMR signal. (A)** Basic level short-axis *in vivo* fusion image of a mouse heart sacrificed at day 21 after immunization. **(B)** The equivalent slice from the 3D *ex vivo* $^{19}$F-CMR. The ventricular cavities have collapsed to a smaller volume, but $^{19}$F signal can still be observed at similar locations as in the *in vivo* image. **(C)** Overview of an HE-stained heart section at the same anatomical level, where the right and left ventricles (RV and LV) can be clearly discerned. **(D&E)** Magnifications of the previous HE-stained heart section. Macrophages can be observed in a thin sub-epicardial layer of the RV myocardium (solid arrow). **(F&G)** CD45 staining in the adjacent heart section confirms the presence of inflammatory bone marrow-derived cells (solid arrow) in the sub-epicardial layer. **(H&I)** F4/80 staining in the adjacent heart section shows the presence of macrophages (solid arrow) at the same anatomical location.

**Figure 6. Immunofluorescence staining of heart sections of EAM mice injected with the dual-mode (A-D) and regular (E-H) emulsion**. **(A)** F4/80 immunostaining of macrophages infiltrates. **(B)** FITC immunostaining indicating the presence of dual-labeled PFC in the same heart section. **(C)** DAPI staining of nuclei. **(D)** Merging of **(A-C)**, where the yellow coloration indicates overlap of F4/80 and FITC staining. **(E-**

**H)** Similar series of staining in an EAM mouse with the regular emulsion (i.e. without FITC). No signal is observed at the FITC frequency (F).

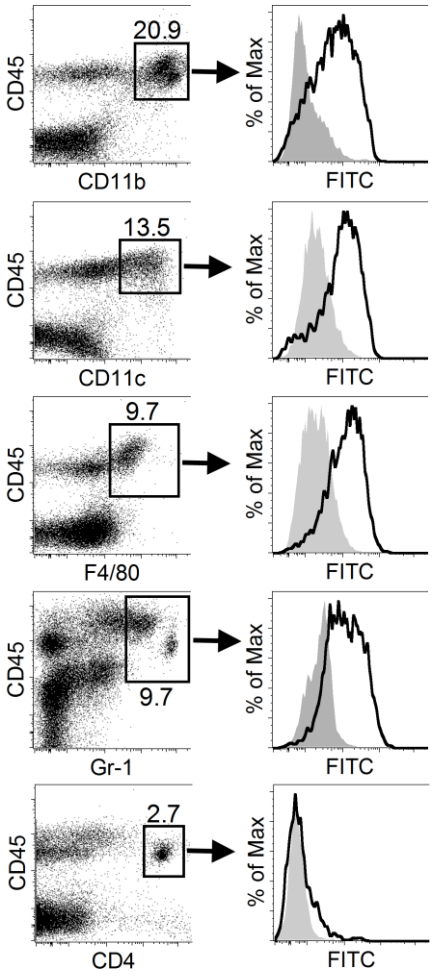


**Figure 7. Flow cytometry profiles of non-myocyte cell fractions isolated from EAM mouse hearts injected with the dual-mode PFC emulsion**. Hearts were isolated at day 21 after immunization and injected with FITC-labeled PFC or PBS. Representative flow cytometry analysis of FITC-positive heart-infiltrating cells gated on the CD45+ cells. The left panels depict CD45 and an immune-cell specific receptor expression (CD11b for monocytes, CD11c for dendritic cells, F4/80 for macrophages, Gr-1 for granulocytes and CD4 for T cells). Gating was performed on double positive populations (black squares with percentage of the total amount of cells), after which the FITC content of these populations is illustrated in the right panels. Histogram plots are shown with the isotype control in gray and the FITC-specific signal as a black line.

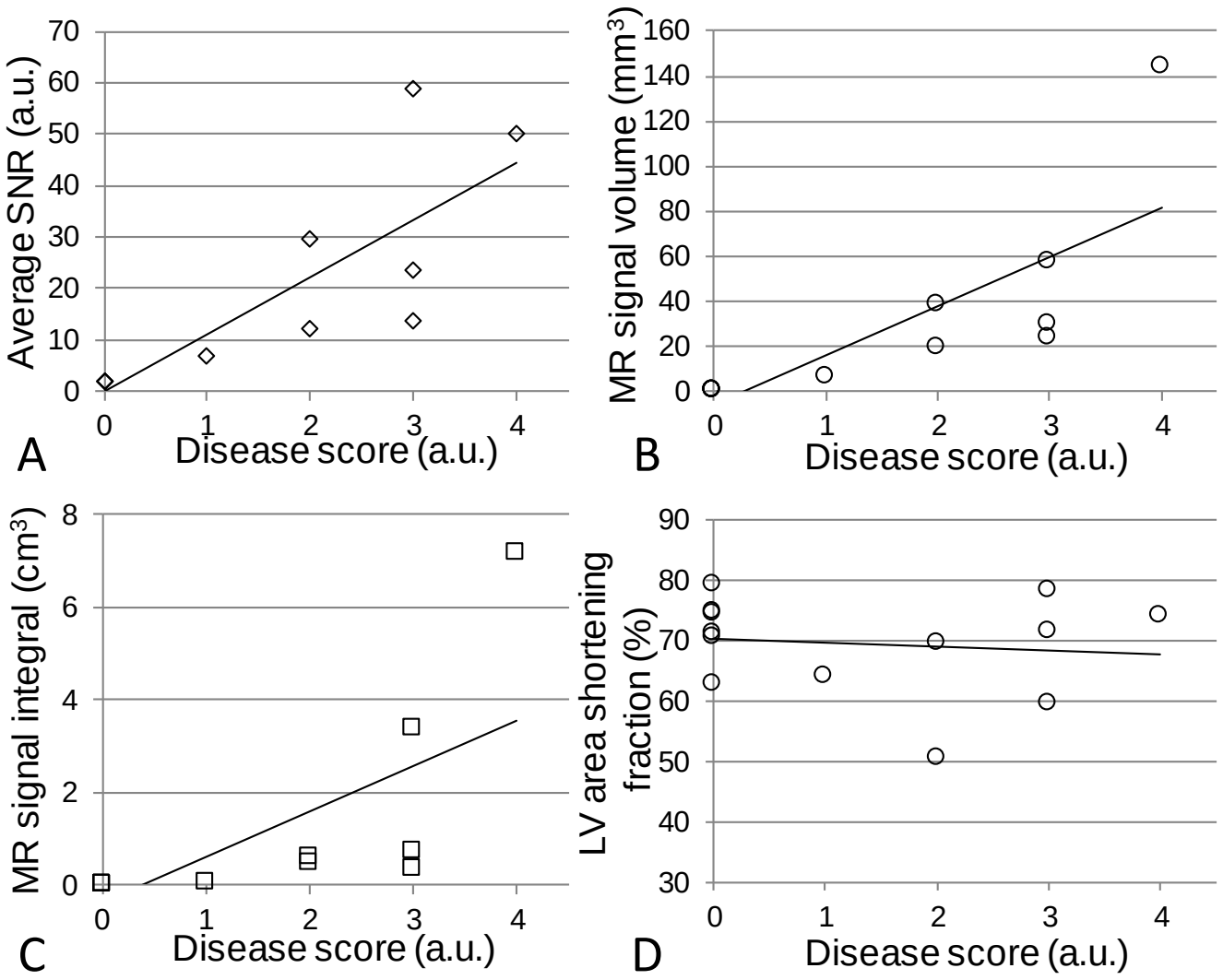


**Figure 8. Correlations of the histological disease score and quantified CMR data**. For these analyses, the EAM mice that received post-mortem histology and PFC(n=7) as well as the healthy controls that received PFC (n=6, overlapping points near the origin) were used. Linear fits were added to illustrate trends. **(A)** The $^{19}$F SNR shows a correlation ($r_s$=0.92, $p$<0.001) with the histological severity of the disease. **(B)** A similar correlation was found for the volume of pixels that had an *in vivo* $^{19}$F MR signal 7 standard deviations above the noise ($Vol_{inflam}$) with the degree of disease severity ($r_s$=0.96, $p$<0.001) and **(C)** with the $^{19}$F signal integral (the product of $Vol_{inflam}$ and the SNR; $r_s$=0.96, $p$<0.001). **(D)** No correlation ($r_s$=-0.14, $p$=0.65) was found between the LV area shortening fraction and the disease score.